energies

MDPI

Article

Application of Promising Electrode Materials in Contact with a Thin-Layer ZrO_2-Based Supporting Electrolyte for Solid Oxide Fuel Cells

Denis A. Osinkin [1,2,*], Ekaterina P. Antonova [1,2], Alena S. Lesnichyova [1,2], Evgeniy S. Tropin [1,2], Mikhail E. Chernov [3], Efim I. Chernov [3], Andrey S. Farlenkov [1,2], Anna V. Khodimchuk [1,2], Vadim A. Eremin [1,2], Anastasia I. Kovrova [1], Anton V. Kuzmin [1,2] and Maxim V. Ananyev [1,2]

1 Institute of High-Temperature Electrochemistry UB RAS, Yekaterinburg 620137, Russia; antonova_ek@list.ru (E.P.A.); a.s.kosykh@mail.ru (A.S.L.); evg2306@mail.ru (E.S.T.); a.farlenkov@yandex.ru (A.S.F.); annlocked@gmail.com (A.V.K.); V-Eremin@list.ru (V.A.E.); kovrova@ihte.uran.ru (A.I.K.); a.v.kuzmin@yandex.ru (A.V.K.); m.ananyev@mail.ru (M.V.A.)

2 Institute of Chemical Engineering, Ural Federal University, Yekaterinburg 620002, Russia

3 "Ekon" Ltd, Obninsk 249037, Russia; chernovm@yandex.ru (M.E.C.); econ@econobninsk.ru (E.I.C.)

* Correspondence: OsinkinDA@mail.ru

Received: 26 December 2019; Accepted: 4 March 2020; Published: 5 March 2020

Abstract: The paper presents the results of an investigation into thin single- and triple-layer ZrO_2-Sc_2O_3-based electrolytes prepared using the tape-casting technique in combination with promising electrodes based on $La_2NiO_{4+\delta}$ and Ni-$Ce_{0.8}Sm_{0.2}O_{2-\delta}$ materials. It is shown that pressing and joint sintering of single electrolyte layers allows multilayer structures to be obtained that are free of defects at the layer interface. Electrical conductivity measurements of a triple-layer electrolyte carried out in longitudinal and transverse directions with both direct and alternating current showed resistance of the interface between the layers on the total resistance of the electrolyte to be minimal. Long-term tests have shown that the greatest degradation in resistance over time occurs in the case of an electrolyte with a tetragonal structure. Symmetrical electrochemical cells with electrodes fabricated using a screen-printing method were examined by means of electrochemical impedance spectroscopy. The polarization resistance of the electrodes was 0.45 and 0.16 Ohm·cm^2 at 800 °C for the fuel and oxygen electrodes, respectively. The distribution of relaxation times method was applied for impedance data analysis. During tests of a single solid oxide fuel cell comprising a supporting triple-layer electrolyte having a thickness of 300 microns, a power density of about 160 mW/cm^2 at 850 °C was obtained using wet hydrogen as fuel and air as an oxidizing gas.

Keywords: thin-layer supporting electrolyte; triple-layer electrolyte; conductivity; DRT; SOFC

1. Introduction

The application of high-temperature solid oxide electrochemical devices presents great opportunities for energy conversion; for example, the use of solid oxide fuel cells (SOFCs) for electricity production [1–5]. In conventional SOFCs, thick layers of Y-doped ZrO_2 electrolyte (YSZ) are used as ionic-conducting materials. However, in this case, a considerable part of the produced energy is lost due to ohmic electrolyte resistance.

One of the most promising approaches to the reduction of ohmic resistance is the application of electrolyte thin films having a thickness of about 10–30 μm [6–8]. Due to technological issues involved in the manufacture of such thin films, their formation should be carried out on a porous supporting substrate (cathode [9–11], anode [12–14], metal interconnector [15–17]) in order to ensure the mechanical strength of the cell. For this reason, questions arise concerning the production technology of supporting

substrates. Another way to reduce ohmic resistance involves the use of thin (150–250 μm) supporting electrolyte layers manufactured from electrolyte materials having a higher ionic conductivity than conventional YSZ—for example, Sc-stabilized ZrO_2 (SSZ). The conductivity of ZrO_2-Sc_2O_3 solid solutions, which reaches a maximum at concentrations of Sc_2O_3 9–12 mol.%, is significantly higher than that of YSZ at similar dopant concentrations [18–20]. However, the cubic ZrO_2-Sc_2O_3 phase is only stable at high temperatures; with a decrease in temperature, it partially transfers to the ordered rhombohedral phase, whose conductivity is much lower [19–21]. For this reason, solid solutions undergo rapid electrical conductivity degradation during long-term testing [21,22]. A common approach to stabilizing the cubic phase in fluorite-like solid solutions containing scandium is to introduce a small amount of yttrium oxide or oxides of other rare earth elements having a large cation radius [19–21]. However, reducing the thickness of the supporting electrolyte also reduces its strength. From this point of view, tetragonal phases based on ZrO_2 are of great interest [23] despite their much lower conductivity. One of the most promising approaches to the creation of a supporting electrolyte membrane combining low resistance with high mechanical strength involves the fabrication of multilayer electrolyte structures combining both cubic and tetragonal phases [23,24].

Other promising approaches to improving the performance of SOFCs include the use of high-efficient electrode materials, e.g., $La_2NiO_{4+\delta}$, which exhibit enhanced performance at low temperatures due to high oxygen exchange and diffusion coefficient values [25–27]; the use of composite electrode materials to extend the electrochemical active zone [28–31]; and the application of two-layered electrode structures (functional and current collector layers) [32–35].

In our study, we attempted to combine two of the above-mentioned approaches, i.e., the application of triple-layer Sc_2O_3-ZrO_2-based electrolytes acting as the supporting SOFC electrolyte with two-layered $La_2NiO_{4+\delta}$-based materials serving as an oxygen electrode. In the present paper, data concerning the functional properties of single- and triple-layer Sc_2O_3-ZrO_2-based electrolytes produced by the tape-casting method are presented along with the results of electrochemical studies for symmetrical cells and SOFCs based thereon.

2. Materials and Methods

The studies were performed on three types of solid electrolyte: a single-layer electrolyte of the composition ZrO_2 + 6 mol.% Sc_2O_3 having a tetragonal structure (hereinafter t.SSZ), a single-layer electrolyte of the composition ZrO_2 + 10 mol.% Sc_2O_3 + 1 mol.% Y_2O_3 with a cubic structure (hereinafter c.SSZ), as well as a triple-layer electrolyte with an internal c.SSZ layer and external t.SSZ layers. For the fabrication of electrolyte layers, single-phase powders of appropriate compositions having a particle size of about 200–500 nm, manufactured by JSC "NeoChem" (Moscow, Russia), were used.

The electrolyte substrates were produced using the tape-casting technique with equipment developed by "Ekon" Ltd, Obninsk, Russia. The formation of a triple-layer structure was carried out by joint pressing of green body layers. The final sintering of the single-layer and triple-layer electrolytes was carried out at 1600 °C. The thickness of the single-layer electrolyte was about 150 μm, while the triple-layer electrolyte had a thickness of around 300 μm.

In order to prevent chemical reactivity between the electrolyte and $La_2NiO_{4+\delta}$-based cathode, a barrier layer of $Ce_{0.8}Sm_{0.2}O_{2-\delta}$ was formed on the surface of the electrolyte by means of the dip-coating method. The final thermal treatment of the samples following dip-coating was performed at a temperature of 1200 °C for 1 h with a heating rate of 50 °C per hour. In order to increase the thickness of the barrier film, the procedure was repeated twice.

The oxygen electrode consisted of two layers: a functional layer having the composition 49 wt.% $La_2NiO_{4+\delta}$ + 49 wt.% $Ce_{0.8}Sm_{0.2}O_{2-\delta}$ + 2 wt.% CuO (LNO-SDC) and a current collector layer with the composition 98 wt.% $LaNi_{0.6}Fe_{0.4}O_{3-\delta}$ + 2 wt.% CuO (LNF). For composite preparation, the $LaNi_{0.6}Fe_{0.4}O_{3-\delta}$, $La_2NiO_{4+\delta}$, and $Ce_{0.8}Sm_{0.2}O_{2-\delta}$ powders were mixed in isopropyl in corresponding ratios. A 56 wt.% NiO + 44 wt.% $Ce_{0.8}Sm_{0.2}O_{2-\delta}$ (NiO-SDC, after reduction Ni-SDC) composite was used as a fuel electrode.

Symmetrical electrochemical cells, as well as fuel cells having planar construction, were prepared using the screen-printing method. The t.SSZ single-layer and t.SSZ/c.SSZ/t.SSZ triple-layer electrolytes were used for electrochemical and fuel cells, respectively. In the case of symmetrical cells, both electrodes were sintered in one step. For fuel cells, the fuel electrode (anode) was initially formed and sintered, then a second step, consisting of oxygen electrode (cathode) preparation, took place. Sintering conditions were 1100 °C for 1 h and 1050 °C for 2 h for the functional and the collector layers of the cathode, respectively; for the anode, sintering took place at 1400 °C for 3 h. In the case of SOFC tests, the electrodes were impregnated with solutions of electrochemically active oxides following sintering. The impregnation procedure was performed with saturated solutions of praseodymium nitrate (for the cathode) and cerium nitrate (for the anode). After impregnation, nitrates were decomposed at 600 °C in air. The content of corresponding oxides in the electrodes following heat treatment was about 1 mg/cm^2.

The phase composition of the materials was verified by X-ray powder diffraction (XRD) in $Cu_{K\alpha}$-radiation ($\lambda(K_{\alpha 1})$ = 1.54 Å) at room temperature in ambient air (D-MAX-2200 RIGAKU). Microstructural investigation was performed using scanning electron microscopy (MIRA 3 LMU, TESCAN) on the cross-sections of the samples. The preparation procedure for the SEM characterization of samples included epoxy impregnation in a vacuum (residual pressure 10^{-2} atm) and polishing. The element composition analysis of ceramic samples was performed by X-ray fluorescence spectroscopy (XRF-1800, Shimadzu). The error in the determination of element concentration did not exceed five relative percent.

The electrical conductivity of electrolyte samples in both transverse and longitudinal directions was measured by two-probe AC and four-probe DC methods, respectively. For this purpose, electrodes made from Pt wire were placed on the electrolyte samples and fixed with Pt paste at a temperature of 1000 °C for 1 h. The complex impedance was measured in the frequency range from 100 mHz to 8 MHz using a Zahner Elektrik IM6 electrochemical analyzer.

Symmetrical electrochemical cells were investigated by impedance spectroscopy (IM6, Zahner, and a Solartron 1260 impedance analyzer with 1287 electrochemical interface). Details of the experimental setup are presented elsewhere [36]. For the distribution of relaxation time (DRT) analysis, a program code, developed by the authors of [37] on the basis of Tikhonov's regularization [38], was applied. For fuel cell studies, the sample was sealed in the measuring cell by high-temperature glass having a transition temperature of 950 °C. Anode reduction was performed at 900 °C in wet hydrogen.

3. Results and Discussion

3.1. Electrolyte Properties

XRD analysis confirmed the absence of impurity phases for all materials under investigation, as well as the absence of chemical reactivity between the components of the used composites (Figure 1) because the diffraction patterns contain reflections only for the studied phases. From the SEM images of the electrolyte surface, it is clearly seen that the samples are dense, with an insignificant number of pores on the surface of the c.SSZ electrolyte (black dots on the surface) and almost no pores on the surface of t.SSZ electrolyte (Figure 2). The average grain size, which does not depend on the electrolyte crystal structure, ranges from 3 to 10 μm. Figure 2 additionally shows a SEM image of the $Ce_{0.8}Sm_{0.2}O_{2-\delta}$ coating on the electrolyte surface. As can be seen, the coating has good adhesion to the electrolyte surface, without any cracks and defects.

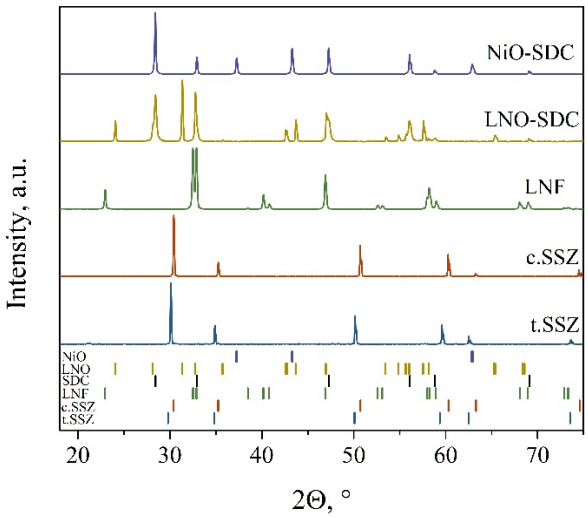

Figure 1. X-ray powder diffraction (XRD) patterns of the electrolyte surface (c.SSZ, t.SSZ) and electrode powders.

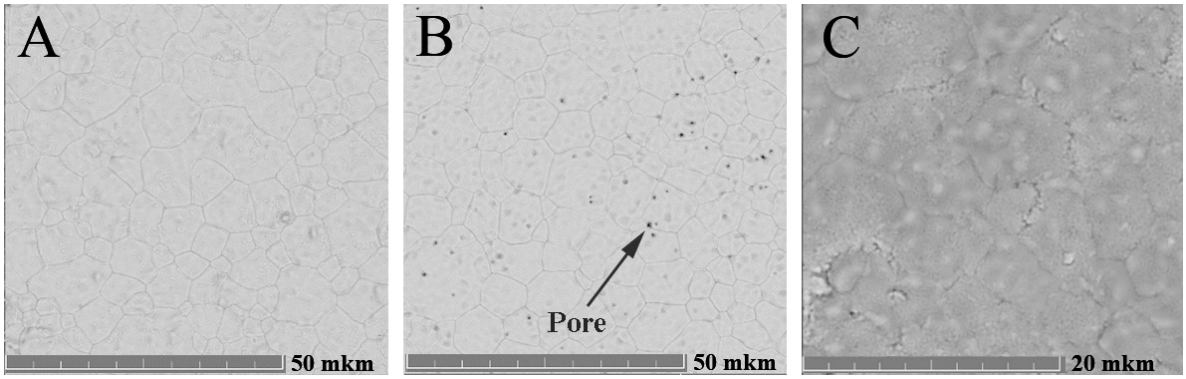

Figure 2. SEM images of the t.SSZ (**A**) and c.SSZ (**B**) electrolyte surfaces and (**C**) $Ce_{0.8}Sm_{0.2}O_{2-\delta}$ coating layer.

Figure 3 shows SEM images with EDX maps (Sc distribution) of the cross-section t.SSZ/c.SSZ/t.SSZ of the triple-layer ceramic before and after long-time high-temperature exposure (850 °C, 1000 h) the results of which will be presented below. As can be seen from the cross-section SEM image for the triple-layered ceramic, there is no through porosity, and the c.SSZ/t.SSZ interfaces have good quality boundaries both before and after long-term tests.

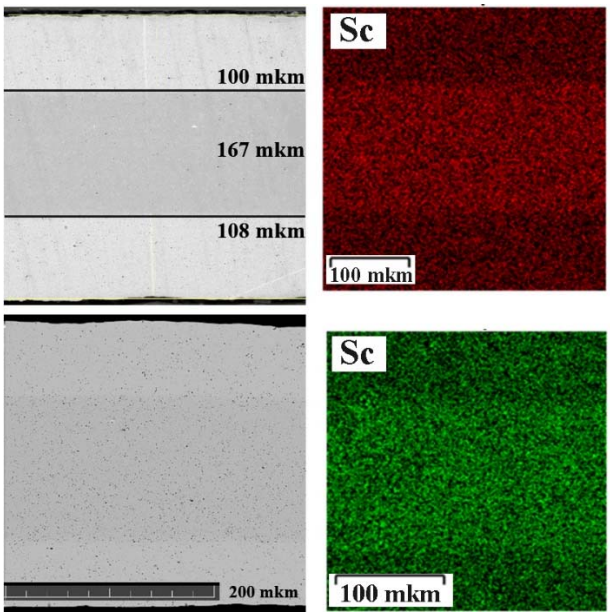

Figure 3. SEM images with EDX maps (Sc distribution) of cross-section t.SSZ/c.SSZ/t.SSZ of triple-layer ceramic before (above) and after (below) long-time high-temperature exposure.

The results of X-ray fluorescence spectroscopy carried out for both electrolytes are presented in Table 1. The obtained values are in good agreement with those obtained from stoichiometric equations, including hafnium and yttrium impurities, which are accompanying elements for zirconium and scandium, respectively. The presence of minute amounts of iron, chromium, and aluminum can be explained by the technological features of ceramics production, such as the usage of alumina balls for powder mixing.

Table 1. Results of X-ray fluorescence spectroscopy analysis of the ceramic samples surface.

t. SSZ		c. SSZ	
ZrO_2	92.93%	ZrO_2	86.66%
Sc_2O_3	6.33%	Sc_2O_3	10.89%
HfO_2	0.56%	HfO_2	0.93%
Y_2O_3	0.12%	Y_2O_3	1.24%
Fe_2O_3	0.06%	$Fe_2O_3/Al_2O_3/Cr_2O_3$	0.04%/0.14%/0.08%

Figure 4a presents the temperature dependencies of the electrical conductivity of the studied electrolytes in the Arrhenius coordinates. No jumps or inflections on the dependencies corresponding to structural changes are observed. The c.SSZ sample possesses the highest electrical conductivity, which is in good agreement with the literature data given in [18–20]. The conductivity of the tetragonal phase is lower, as expected [23], and the conductivity of a three-layer ceramic has an average value compared to t.SSZ and c.SSZ. Figure 4a also shows the conductivity values measured by the impedance method. DC and AC conductivities are well comparable in overlapping temperature ranges. Typical impedance spectra for materials under study at 500 °C are presented in Figure 4b. As could be seen, the EIS spectra of single-layer structures are fitted by two RQ elements. The first RQ1 corresponds to the electrolyte with the value of capacitance about 10^{-10} F/cm^2, and the second RQ2 corresponds to the electrode process with the value of capacitance about 10^{-6} F/cm^2. Additional DC four-probe measurements demonstrate that resistivity of the whole sample is described by the first semicircle, meaning that the second one should be ascribed to the electrode process. Moreover, bulk and grain

boundary resistances could not be accurately estimated from the first semicircle of the spectrum. This may be due to the slightly distinguishable composition of the bulk and grain boundaries, as well as the large grain size (≈10 μm) of ceramics, which leads to the low resistance of grain boundaries. At the same time, the EIS spectrum for the t.SSZ/c.SSZ/t.SSZ electrolyte is similar to ones of single-layer structures, which indicates the absence of additional relaxation processes (semicircles) due to resistance at the t.SSZ/c.SSZ interfaces of a three-layer electrolyte. A comparison of the conductivity values for scandium-containing materials and YSZ [24] demonstrate a significant advantage of the former one for application as electrolytes for SOFCs.

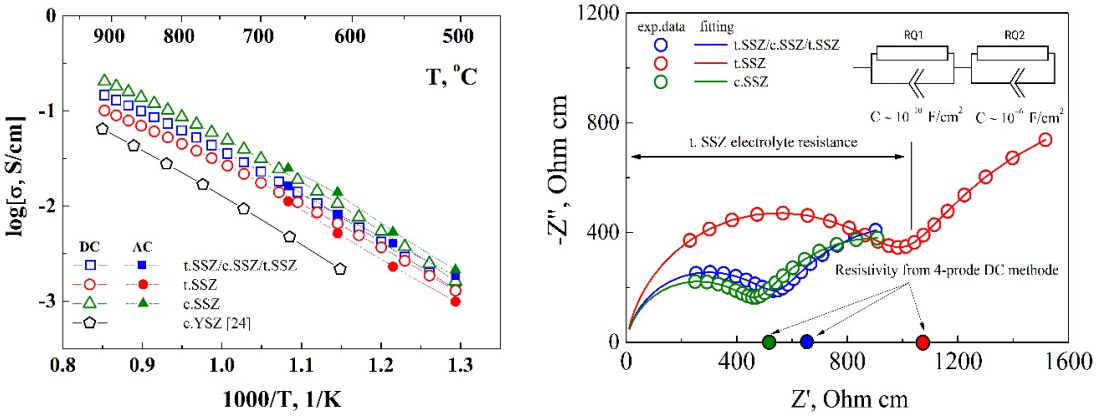

Figure 4. Temperature dependencies of electrical conductivities for SSZ ceramics obtained by four-probe DC and two-probe AC methods (**left**) and EIS spectra recorded at 500 °C (**right**).

During the long-term electrolyte resistance stability tests, the largest increase in resistance was found for t.SSZ, at around 14.6% per 1000 h (Figure 5). For the c.SSZ sample, the resistance value increases by 7.4% over the same period. The relative increase in resistance for a triple-layer electrolyte, which amounts to 11.6% per 1000 h, is mainly associated with the degradation of the tetragonal phase. The degradation mechanism of electrolytes based on zirconium oxide is usually associated with the formation of poorly conducting low-symmetric phases [19,23]. No changes in the phase composition were visible in the X-ray phase analysis of the samples following degradation, probably due to their low content. The element distribution maps for a triple-layer sample show that there is no noticeable redistribution of scandium cations in layers with different contents during a long exposure (Figure 3). The nature of the time dependencies does not differ from those given in the literature [19,22,24]. Over time, the degradation rate slows down over time significantly. A simple equation has been proposed [22] to describe the degradation process:

$$R_\tau = R_0 + B\tau^{1/2},$$

where R_0, R_τ are the resistivities of the electrolyte prior to degradation, at the instant of time τ, respectively; B is a constant. By extrapolating the time dependencies, according to this equation, we are able to predict that the increase in the resistance of a triple-layer electrolyte will not exceed 17% and 23% after 10,000 and 50,000 h, respectively

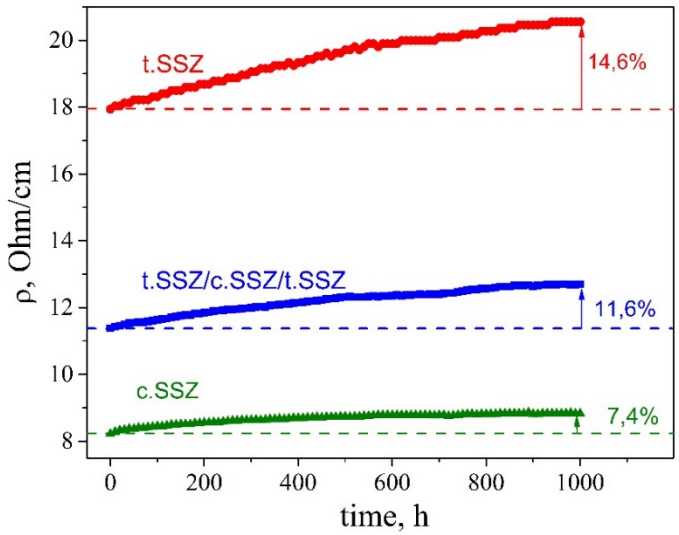

Figure 5. Long-term tests of electrolytes at 850 °C.

3.2. Electrochemical Cells and Performance

The electrochemical activity of the electrodes in contact with the t.SSZ electrolyte was investigated on the symmetrical electrochemical cells. Measurements were conducted in the temperature range 750–850 °C in an air atmosphere for the LNO-SDC/LNF oxygen electrode; for the Ni-SDC fuel electrode, measurements were carried out in the temperature range 650–850 °C in wet (pH_2O = 0.03 atm) hydrogen. Figure 6 presents the comparison between the values of ohmic resistance of the symmetrical electrochemical cells, as extracted from the impedance spectra, and the electrolyte resistance values for t.SSZ as determined by the four-probe DC method. It can be seen that the values obtained using the different measurement techniques, as well as the apparent activation energy values for electrolyte conductivity, are in good agreement. The closeness of the values of the electrolyte resistance and the activation energy obtained by two different methods indicate the absence of chemical interaction between the electrode and electrolyte materials.

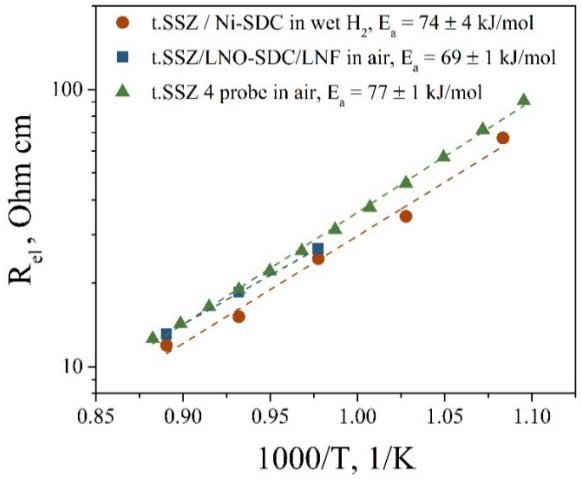

Figure 6. Temperature dependencies of electrolyte resistance obtained from impedance spectra and four-probe DC methods.

Temperature dependencies of polarization resistance for the investigated electrodes are presented in Figure 7. At 800 °C, the polarization resistance (R_η) of the oxygen electrode is about 0.16 Ω·cm^2, with an apparent activation energy (E_a) of about 130 kJ/mol. The obtained value of E_a is close to those

obtained in [39,40] for similar oxygen double-layer electrodes. Polarization resistance values for the fuel electrode are somewhat higher than those for the oxygen electrode; at 800 °C, the value was around 0.45 Ω·cm^2. The apparent activation energy value is about 85 kJ/mol, with such values being quite typical for Ni-SDC electrodes [41].

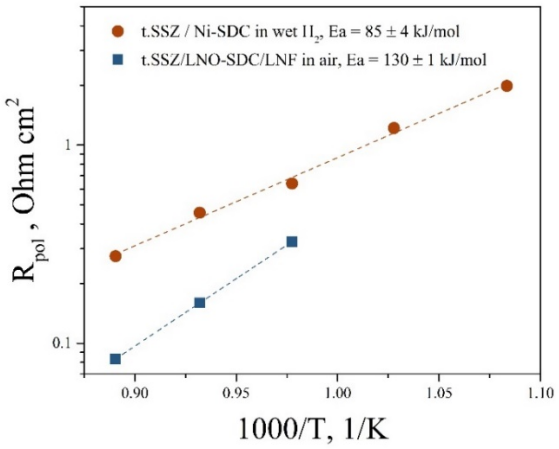

Figure 7. Temperature dependencies of electrodes' polarization resistance.

Impedance spectra for symmetrical electrochemical cells are depicted in Figure 8A,B. For their analysis, the distribution of relaxation times method (DRT) was applied, as it has much higher resolution in comparison to traditional complex nonlinear squares method [42,43]. DRT functions calculated from impedance data are presented in Figure 8C,D. It can be seen that, for oxygen electrodes, the functions consist of several processes. The low-frequency step can be assigned to the gas diffusion [25], while the three steps in the middle-frequency region have been recently identified in [44] as oxygen ion diffusion on the electrode/electrolyte interface, charge transfer in the adsorption layer, and oxygen surface exchange and diffusion in the electrode material.

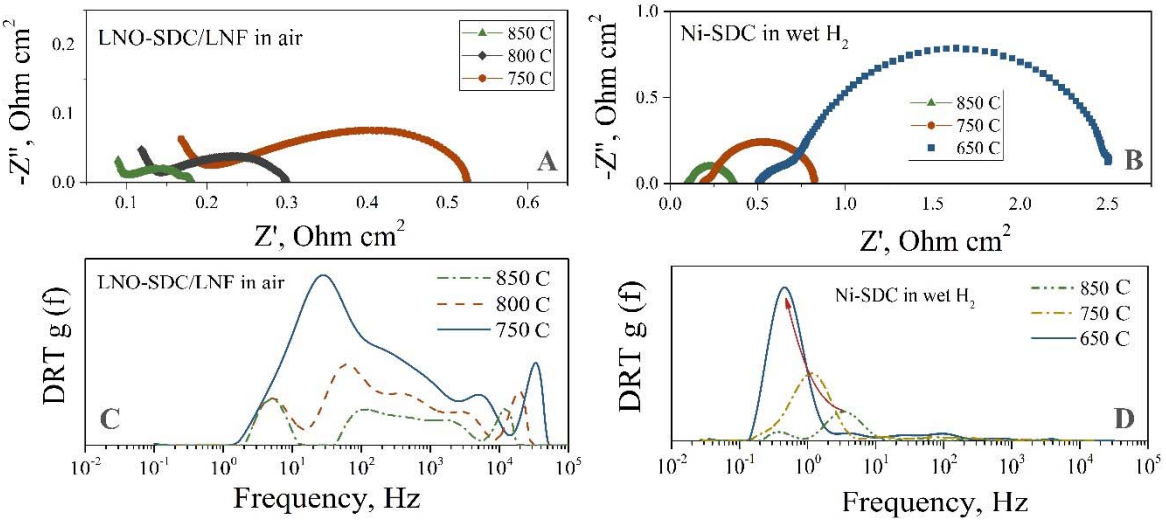

Figure 8. Impedance spectra for symmetric electrochemical cells with t.SSZ electrolyte (**A**,**B**) and distribution of relaxation time (DRT) functions, calculated from impedance spectra (**C**,**D**).

For fuel electrodes, two peaks at the frequencies of 0.3 and 5 Hz can be found at the DRT function at 600 °C. While the temperature increases the DRT function becomes more complicated. At 850 °C three peaks at the DRT function can be identified at 0.3, 5, and 100 Hz. Similar behavior for the DRT function has been observed previously in [45] for Ni-SDC anodes. Based on the results, obtained in [44]

we can conclude that the rate of the hydrogen oxidation is limited by oxygen ionic diffusion in SDC, reactions between adsorbed forms of the potential determining particles on the anode surface as well as the gas diffusion.

The cross-section fuel cell SEM image and SOFC test results are shown in Figure 9. In the temperature range 750–850 °C and using wet hydrogen as a fuel gas, the power density was about 90–160 mW/cm^2, respectively. To our knowledge, there is no literary data concerning SOFCs with a 300 μm electrolyte and an LNO-based cathode. However, we can compare our results with those for similar electrolyte-supported SOFCs. For example, in [46] power densities of about 160–270 mW/cm^2 were obtained at 800 °C for the SOFC with a 270 μm YSZ electrolyte, two-layer LSM/LSM-YSZ cathode, and Ni-YSZ anode, which is close to our values. The obtained power values are not very high, probably due to the ohmic resistance of the t.SSZ/c.SSZ/t.SSZ electrolyte. Reducing the thickness of the electrolyte will significantly increase the power performance of the SOFC.

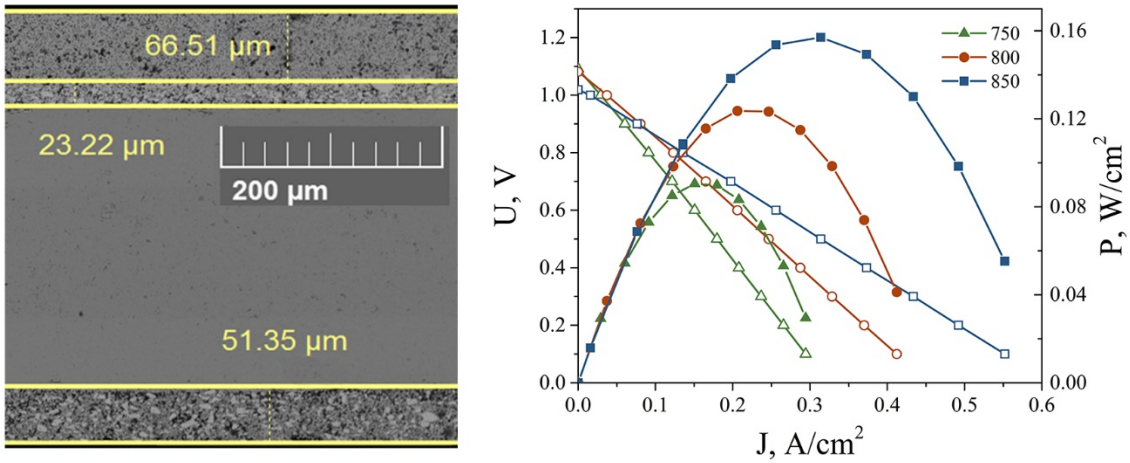

Figure 9. SEM image of fuel cell cross-section and performances of solid oxide fuel cells (SOFC).

4. Conclusions

ZrO_2-Sc_2O_3-based electrolytes were studied, both in the form of single-layers having a thickness of about 150 μm, and as triple-layer samples with a combined thickness of 300 μm. It is shown that in the case of the triple-layer electrolytes, the resistance of the layer interface does not significantly affect the total resistance. Long-term tests of the electrolytes were carried out at 850 °C for 1000 h. It was found that the resistance of the electrolyte having a tetragonal structure degrades most rapidly, exhibiting a relative increase in resistance of about 15% after 1000 testing hours. For an electrolyte with a cubic structure, the change in resistance was about 7% per 1000 h. The high performance of electrode materials based on $La_2NiO_{4+\delta}$ (with a barrier SDC layer) and Ni-SDC in contact with an electrolyte with a tetragonal structure is demonstrated. Single fuel cells having a triple-layer 300 μm thick supporting electrolyte were studied. The resulting power density amounts to 160 mW/cm^2 at 850 °C.

Author Contributions: Conceptualization, D.A.O., M.V.A., and A.V.K. (Anton V. Kuzmin); methodology, E.S.T., M.E.C., E.I.C., and A.I.K.; validation, A.V.K. (Anton V. Kuzmin), M.V.A. and D.A.O.; formal analysis, D.A.O., E.P.A., and A.S.L.; investigation, D.A.O., E.P.A., A.S.L., A.S.F., A.V.K. (Anna V. Khodimchuk), and V.A.E.; writing—original draft preparation, D.A.O., E.P.A., and A.S.L.; writing—review and editing, D.A.O., E.P.A., and A.V.K. (Anton V. Kuzmin); visualization, D.A.O., E.P.A., and A.S.L.; project administrator, M.V.A. and E.I.C. All authors have read and approved the final manuscript.

Funding: The study was partly financially supported by the Russian Foundation for Basic Research (17-08-01227), Russian Federation Government, agreement 02.A03.21.0006 (No. 211) and "InEnergy" LTD agreement of 2018.

Acknowledgments: This work was partly carried out using facilities of the shared access center 'Composition of Compounds' IHTE, UB RAS. The authors are grateful to A.E. Dosovitskiy "NeoChem" (Moscow, Russia) for provided powders of solid electrolytes based on zirconium oxide.

Conflicts of Interest: The authors declare no conflict of interest.

References

1. Chen, D.; Hu, B.; Ding, K.; Yan, C.; Lu, L. The geometry effect of cathode/anode areas ratio on electrochemical performance of button fuel cell using mixed conducting materials. *Energies* **2018**, *11*, 1875. [CrossRef]
2. Mantelli, L.; De Campo, M.; Ferrari, M.L.; Magistri, L. Fuel flexibility for a turbocharged SOFC system. *Energy Procedia* **2019**, *158*, 1974–1979. [CrossRef]
3. Nguyen, X.-V.; Chang, C.-T.; Jung, G.-B.; Chan, S.-H.; Huang, W.C.-W.; Hsiao, K.-J.; Lee, W.-T.; Chang, S.-W.; Kao, I.-C. Effect of sintering temperature and applied load on anode-supported electrodes for SOFC application. *Energies* **2016**, *9*, 701. [CrossRef]
4. López-Robledo, M.J.; Laguna-Bercero, M.A.; Larrea, A.; Orera, V.M. Reversible operation of microtubular solid oxide cells using $La_{0.6}Sr_{0.4}Co_{0.2}Fe_{0.8}O_{3-\delta}$-$Ce_{0.9}Gd_{0.1}O_{2-\delta}$ oxygen electrodes. *J. Power Sources* **2018**, *378*, 184–189. [CrossRef]
5. Fernandes, M.D.; de Andrade, S.T.P.; Bistritzki, V.N.; Fonseca, R.M.; Zacarias, L.G.; Gonçalves, H.N.C.; de Castro, A.F.; Domingues, R.Z.; Matencio, T. SOFC-APU systems for aircraft: A review. *Int. J. Hydrog. Energy* **2018**, *43*, 16311–16333. [CrossRef]
6. Oskouyi, O.E.; Shahmiri, M.; Maghsoudipour, A.; Hasheminiasari, M. Pulsed constant voltage electrophoretic deposition of YSZ electrolyte coating on conducting porous Ni–YSZ cermet for SOFCs applications. *J. Alloys Compd.* **2019**, *785*, 220–227. [CrossRef]
7. Jafari, M.; Salamati, H.; Zhiani, M.; Shahsavari, E. Enhancement of an IT-SOFC cathode by introducing YSZ: Electrical and electrochemical properties of $La_{0.6}Ca_{0.4}Fe_{0.8}Ni_{0.2}O_{3-\delta}$-YSZ composites. *Int. J. Hydrog. Energy* **2019**, *44*, 1953–1966. [CrossRef]
8. Park, J.M.; Kim, D.Y.; Baek, J.D.; Yoon, Y.-J.; Su, P.-C.; Lee, S.H. Numerical study on electrochemical performance of low-temperature micro-solid oxide fuel cells with submicron platinum electrodes. *Energies* **2018**, *11*, 1204. [CrossRef]
9. Beresnev, S.M.; Bobrenok, O.F.; Kuzin, B.L.; Bogdanovich, N.M.; Kurteeva, A.A.; Osinkin, D.A.; Vdovin, G.K.; Bronin, D.I. Single fuel cell with supported LSM cathode. *Rus. J. Electrochem.* **2012**, *48*, 969–997. [CrossRef]
10. Lin, Q.; Lin, J.; Liu, T.; Xia, C.; Chen, C. Solid oxide fuel cells supported on cathodes with large straight open pores and catalyst-decorated surfaces. *Solid State Ion.* **2018**, *323*, 130–135. [CrossRef]
11. Rehman, S.U.; Song, R.-H.; Lee, J.-W.; Lim, T.-H.; Park, S.-J.; Lee, S.-B. Effect of GDC addition method on the properties of LSM–YSZ composite cathode support for solid oxide fuel cells. *Ceram. Int.* **2016**, *42*, 11772–11779. [CrossRef]
12. Kurteeva, A.A.; Beresnev, S.M.; Osinkin, D.A.; Kuzin, B.L.; Vdovin, G.K.; Zhuravlev, V.D.; Bogdanovich, N.M.; Bronin, D.I.; Pankratov, A.A.; Yaroslavtsev, I.Y. Single solid–oxide fuel cells with supporting Ni-cermet anode. *Rus. J. Electrochem.* **2011**, *47*, 1381–1388. [CrossRef]
13. Osinkin, D.A.; Bogdanovich, N.M.; Beresnev, S.M.; Zhuravlev, V.D. High-performance anode-supported solid oxide fuel cell with impregnated electrodes. *J. Power Sources* **2015**, *288*, 20–25. [CrossRef]
14. Timurkutluk, B.; Celik, S.; Ucar, E. Influence of doctor blade gap on the properties of tape cast NiO/YSZ anode supports for solid oxide fuel cells. *Ceram. Int.* **2019**, *45*, 3192–3198. [CrossRef]
15. Choi, H.-J.; Kim, T.W.; Na, Y.-H.; Seo, D.-W.; Woo, S.-K.; Huh, J.-Y.; Kim, S.-D. Enhanced electrochemical performance of metal-supported solid oxide fuel cells via an inner coating of $Gd_{0.1}Ce_{0.9}O_{2-\delta}$ nanosol in the porous NiFe-metal support. *J. Power Sources* **2018**, *406*, 81–87. [CrossRef]
16. Tucker, M.C. Dynamic-temperature operation of metal-supported solid oxide fuel cells. *J. Power Sources* **2018**, *395*, 314–317. [CrossRef]
17. Shah, M.; Das, S.; Nayak, A.K.; Mondal, P.; Bordoloi, A. Smart designing of metal-support interface for imperishable dry reforming catalyst. *Appl. Catal. A: Gen.* **2018**, *556*, 137–154. [CrossRef]
18. Liu, T.; Zhang, X.; Wang, X.; Yu, J.; Li, L. A review of zirconia-based solid electrolytes. *Ionics* **2016**, *22*, 2249–2262. [CrossRef]
19. Omar, S.; Najib, W.B.; Chen, W.; Bonanos, N. Electrical Conductivity of 10 mol% Sc_2O_3–1 mol% M_2O_3–ZrO_2 Ceramics. *J. Am. Ceram. Soc.* **2012**, *95*, 1965–1972. [CrossRef]

20. Norberg, S.T.; Hull, S.; Ahmed, I.; Eriksson, S.G.; Marrocchelli, D.; Madden, P.A.; Li, P.; Irvine, J.T.S. Structural disorder in doped zirconias, Part I: The $Zr_{0.8}Sc_{0.2-x}Y_xO_{1.9}$ ($0.0 \leq x \geq 0.2$) System. *Chem. Mater.* **2011**, *23*, 1356–1364. [CrossRef]
21. Irvine, J.T.S.; Politova, T.; Kruth, A. Yttria co-doping of Scandia-zirconia electrolytes for SOFCs. *Proc. Electrochem. Soc.* **2005**, *PV 2005-07*, 941–946. [CrossRef]
22. Vlasov, A.N.; Perfiliev, M.V. Ageing of ZrO_2-based solid electrolytes. *Solid State Ion.* **1987**, *25*, 245–253. [CrossRef]
23. Seabaugh, M.M.; Day, M.J.; Sabolsky, K.; Ibanez, S.; Swartz, S.L. Materials and components for solid oxide fuel cells systems. *Proc. Electrochem. Soc.* **2005**, *PV 2005-07*, 1037–1044. [CrossRef]
24. Kuzmin, A.V.; Novikova, Y.V.; Stroeva, A.Y.; Gorelov, V.P.; Vylkov, A.I.; Ananiev, M.V.; Ermakov, A.V.; Zaikov, Y.P. Formation and properties of a support made of solid solutions based on zirconium oxide for single tubular solid-oxide fuel cells. *Rus. J. Appl. Chem.* **2018**, *91*, 196–201. [CrossRef]
25. Antonova, E.P.; Osinkin, D.A.; Bogdanovich, N.M.; Gorshkov, M.Y.; Bronin, D.I. Electrochemical performance of $Ln_2NiO_{4+\delta}$ (Ln–La, Nd, Pr) and $Sr_2Fe_{1.5}Mo_{0.5}O_{6-\delta}$ oxide electrodes in contact with apatite-type $La_{10}(SiO_6)_4O_3$ electrolyte. *Solid State Ion.* **2019**, *329*, 82–89. [CrossRef]
26. Benamira, M.; Ringuedé, A.; Cassir, M.; Horwat, D.; Lenormand, P.; Ansart, F.; Bassat, J.M.; Viricelle, J.P. Enhancing oxygen reduction reaction of YSZ/$La_2NiO_{4+\delta}$ using an ultrathin $La_2NiO_{4+\delta}$ interfacial layer. *J. Alloy. Compd.* **2018**, *746*, 413–420. [CrossRef]
27. Ananyev, M.V.; Tropin, E.S.; Eremin, V.A.; Farlenkov, A.S.; Smirnov, A.S.; Kolchugin, A.A.; Porotnikova, N.M.; Khodimchuk, A.V.; Berenov, A.V.; Kurumchin, E.K. Oxygen isotope exchange in $La_2NiO_{4\pm\delta}$. *Phys. Chem. Chem. Phys.* **2016**, *18*, 9102–9111. [CrossRef]
28. Xu, J.; Zhou, X.; Dong, X.; Pan, L.; Sun, K. Catalytic activity of infiltrated $La_{0.3}Sr_{0.7}Ti_{0.3}Fe_{0.7}O_{3-\delta}$–$CeO_2$ as a composite SOFC anode material for H_2 and CO oxidation. *Int. J. Hydrog. Energy* **2017**, *42*, 15632–15640. [CrossRef]
29. Osinkin, D.A.; Lobachevskaya, N.I.; Suntsov, A.Y. The electrochemical behavior of the promising $Sr_2Fe_{1.5}Mo_{0.5}O_{6-\delta}$ + $Ce_{0.8}Sm_{0.2}O_{1.9-\delta}$ anode for the intermediate temperature solid oxide fuel cells. *J. Alloy. Compd.* **2017**, *708*, 451–455. [CrossRef]
30. Khaerudini, D.S.; Guan, G.; Zhang, P.; Hao, X.; Wang, Z.; Xue, C.; Kasai, Y.; Abudula, A. Performance assessment of $Bi_{0.3}Sr_{0.7}Co_{0.3}Fe_{0.7}O_{3-\delta}$-LSCF composite as cathode for intermediate-temperature solid oxide fuel cells with $La_{0.8}Sr_{0.2}Ga_{0.8}Mg_{0.2}O_{3-\delta}$ electrolyte. *J. Power Sources* **2015**, *298*, 269–279. [CrossRef]
31. Nielsen, J.; Jacobsen, T.; Wandel, M. Impedance of porous IT-SOFC LSCF:CGO composite cathodes. *Electrochim. Acta* **2011**, *56*, 7963–7974. [CrossRef]
32. Dierickx, S.; Mundloch, T.; Weber, A.; Ivers-Tiffée, E. Advanced impedance model for double-layered solid oxide fuel cell cermet anodes. *J. Power Sources* **2019**, *415*, 69–82. [CrossRef]
33. Yin, Y.; Li, S.; Xia, C.; Meng, G. Electrochemical performance of IT-SOFCs with a double-layer anode. *J. Power Sources* **2007**, *167*, 90–93. [CrossRef]
34. Tao, Y.; Nishino, H.; Ashidate, S.; Kokubo, H.; Watanabe, M.; Uchida, H. Polarization properties of $La_{0.6}Sr_{0.4}Co_{0.2}Fe_{0.8}O_3$-based double layer-type oxygen electrodes for reversible SOFCs. *Electrochim. Acta* **2009**, *54*, 3309–3315. [CrossRef]
35. Marinha, D.; Hayd, J.; Dessemond, L.; Ivers-Tiffée, E.; Djurado, E. Performance of (La,Sr)(Co,Fe)O_{3-x} double-layer cathode films for intermediate temperature solid oxide fuel cell. *J. Power Sources* **2011**, *196*, 5084–5090. [CrossRef]
36. Osinkin, D.A.; Kuzin, B.L. Hydrogen oxidation kinetics at Ni–$Zr_{0.9}Sc_{0.1}O_{1.95}$ anode: Influence of the difference of potential in the dense part of the double electric layer. *Electrochim. Acta* **2018**, *282*, 128–136. [CrossRef]
37. Gavrilyuk, A.L.; Osinkin, D.A.; Bronin, D.I. The use of Tikhonov regularization method for calculating the distribution function of relaxation times in impedance spectroscopy. *Rus. J. Electrochem.* **2017**, *53*, 575–588. [CrossRef]
38. Tikhonov, A.N.; Arsenin, V.Y. *Solution of Ill-posed Problems*; Winston & Sons: Washington, DC, USA, 1977.
39. Pikalova, E.Y.; Bogdanovich, N.M.; Kolchugin, A.A.; Ananyev, M.V.; Pankratov, A.A. Influence of the synthesis method on the electrochemical properties of bilayer electrodes based on $La_2NiO_{4+\delta}$ and $LaNi_{0.6}Fe_{0.4}O_{3-\delta}$. *Solid State Ion.* **2016**, *288*, 36–42. [CrossRef]

40. Pikalova, E.Y.; Bogdanovich, N.M.; Kolchugin, A.A.; Osinkin, D.A.; Bronin, D.I. Electrical and electrochemical properties of $La_2NiO_{4+\delta}$—based cathodes in contact with $Ce_{0.8}Sm_{0.2}O_{2-\delta}$ electrolyte. *Procedia Eng.* **2014**, *98*, 105–110. [CrossRef]
41. Chen, M.; Kim, B.H.; Xu, Q.; Ahn, B.G. Preparation and electrochemical properties of Ni–SDC thin films for IT-SOFC anode. *J. Membr. Sci.* **2009**, *334*, 138–147. [CrossRef]
42. Boukamp, B.A. Fourier transform distribution function of relaxation times; application and limitations. *Electrochim. Acta* **2015**, *154*, 35–46. [CrossRef]
43. Saccoccio, M.; Wan, T.H.; Chen, C.; Ciucci, F. Optimal regularization in distribution of relaxation times applied to electrochemical impedance spectroscopy: Ridge and lasso regression methods—A theoretical and experimental study. *Electrochim. Acta* **2014**, *147*, 470–482. [CrossRef]
44. Antonova, E.P.; Khodimchuk, A.V.; Usov, G.R.; Tropin, E.S.; Farlenkov, A.S.; Khrustov, A.V.; Ananyev, M.V. EIS analysis of electrode kinetics for $La_2NiO_{4+\delta}$ cathode in contact with $Ce_{0.8}Sm_{0.2}O_{1.9}$ electrolyte: From DRT analysis to physical model of the electrochemical process. *J. Solid State Electrochem.* **2019**, *23*, 1279–1287. [CrossRef]
45. Osinkin, D.A. Complementary effect of ceria on the hydrogen oxidation kinetics on Ni—$Ce_{0.8}Sm_{0.2}O_{2-\delta}$ anode. *Electrochim. Acta* **2020**, *330*, 135257. [CrossRef]
46. Timurkutluk, B.; Dokuyucu, S. The role of tape thickness on mechanical properties and performance of electrolyte supports in solid oxide fuel cells. *Ceram. Int.* **2018**, *44*, 17399–17406. [CrossRef]